State dependent δ-pairing force with Nilsson models: Nuclear shapes, radii, and masses

Kamila Sieja* and Andrzej Baran†
Institute of Physics UMCS, 20-031 Lublin, Poland
(Received 20 December 2002; published 15 October 2003)

The single particle Nilsson as well as Nilsson-Seo-type potentials and the state dependent δ-pairing force are used to calculate nuclear deformations, root-mean square charge radii, quadrupole moments, and masses of rare earth nuclei. The masses are evaluated by means of Strutinsky shell correction method where the macroscopic part of the energy is the recently developed Lublin-Skrasbourg drop model and the microscopic energy is the sum of shell and pairing corrections. The latter is based on the δ-force pairing interaction, the strength of which is adjusted to the three-mass pairing indicators $\Delta^{(3)}$ calculated from the experimental nuclear masses. The results are compared to experimental data and to estimates done in other models. The agreement of our results with the measured data is acceptable. The standard deviation for calculated masses is about 0.8 MeV. The results show that the state dependent δ-pairing force works similarly as in the monopole pairing models.

DOI: 10.1103/PhysRevC.68.044308 PACS number(s): 21.10.Dr, 21.10.Ft, 21.10.Gv, 21.30.Fe

I. INTRODUCTORY REMARKS

Historically, the Nilsson potential [1,2] was introduced as the first phenomenological single particle model taking into account nuclear deformations. Algorithms using Nilsson model are faster and more effective than those using, e.g., Hartree-Fock approximation, especially in cases where one has to calculate fission barriers and mass parameters.

Methods based on self-consistent calculations such as Skyrme-Hartree-Fock or Hartree-Fock-Bogoliubov are very effective in ground state calculations and rather cumbersome otherwise. At the same time the results obtained by Strutinsky shell correction method [3–5] and the BCS model are comparable to the realistic ones. The Nilsson-type models seem to work well also in cases of β-unstable nuclei very far from the nuclear β-stability line.

There are many examples of a successful use of the Nilsson-type potentials, e.g., in Ref. [6,7] where nuclear properties are calculated throughout the periodic system to a very good accuracy.

To understand and to determine basic nuclear excitations and the stability properties of the nuclei especially in case of nuclei far from the β-stability line where the emission of single particles as well as the pair of particles is observed [8], the knowledge of the pairing force is crucial. It is a phenomenon responsible for pair formation and its transfer (collective pairing vibrations and rotations) and pair breaking. Such phenomena are observed in radioactive nuclear beam facilities [8].

Both the δ function and the pairing force are intended to represent the short range component of nuclear interaction. As shown in, e.g., Ref. [9] the empirical level schemes of two-particle states in magic nuclei such as ^{210}Po, ^{210}Pb show that the δ interaction reproduces empirical spectra more accurately. The same is true for magic nuclei, such as Sn isotopes.

The common features of both interactions monopole pairing and δ suggest to use the latter as a particle-particle channel force instead of the monopole pairing interaction. The expansion of the δ interaction shows a clear multipole nature. Besides the constant monopole term it contains all even multipoles. The quadrupole-pairing interaction added to the monopole pairing Hamiltonian was already studied in particle-vibrational model of Bes and Broglia [10,11] or in the analysis of the staggering of nuclear radii [12]. As was shown, e.g., in Ref. [13], the isovector quadrupole pairing is important to shift the rotational alignment in the rare earth region and clarifies the signature inversion effect in some nuclei [14]. The research concerning the state dependent δ pairing which contains all of the multipoles of the pairing field seems therefore to be interesting and it might help in clarifying the mentioned phenomena.

Primarily, the state dependent pairing was used in Hartree-Fock-Bogoliubov calculations with Skyrme forces [15] and later on also in relativistic mean field models (RMF) where the authors treat the pairing in the framework of Bogoliubov theory [16–18]. The Skyrme models using the δ-pairing-type BCS were also used to calculate the nuclear collective 2^+ and higher angular momentum states [19–21].

The results of such theories are comparable to the Strutinsky-type calculations in case of the nuclei very close to the nuclear stability line. The predicted nuclear masses and rms calculated in the framework of the Skyrme-Hartree-Fock model with the δ-pairing force are very precise. The rms deviation for the mass is close to 0.7 MeV in the ETFSI model [22,23] or even less in HFBCS-1 model [24,25] and the rms deviation for the charge radii is 0.024 fm [26].

The macroscopic part of the nuclear energy was recently reinvestigated in Ref. [27] where instead of the standard macroscopic energy as discussed, e.g., in Refs. [28,29] the authors used the new curvature dependent liquid drop formula, the so called Lublin-Strasbourg drop (LSD). Masses, fission half-lives or Q_α values calculated using LSD are in a very good agreement with experimental data [30].

The Strutinsky methods are very convenient in calculations of the total nuclear energy surfaces, fission barriers,

*Email address: ksieja@hektor.umcs.lublin.pl
†Email address: baran@tytan.umcs.lublin.pl

high spin properties, in shape-isomerism studies, and excited particle-hole configurations. On the other hand, the self-consistent methods are extremely useful in the detailed theoretical description of the nuclear states, the global features of which are already known.

The subject of the present paper is to calculate the masses and the nuclear charge radii using the Nilsson potential and the Strutinsky approach where the pairing energy is determined in the BCS state dependent pairing model with the δ-type interaction and the macroscopic part of energy is LSD.

The paper is organized as follows. In Sec. II we remind very shortly the main features of Nilsson and Nilsson-Seo potentials. Section III is devoted to $\delta(\vec{r}_{12})$ pairing forces and to the way of treating the corresponding BCS equations. Section IV describes the recent macroscopic nuclear drop model, LSD, [27] which takes into account the curvature term proposed originally in the nuclear liquid droplet model by Myers and Swiatecki [29,31]. In Sec. V the rms charge nuclear radii are discussed. And finally in Sec. VI we discuss the results of our calculations: matrix elements of the state dependent δ-pairing interaction, strengths V_0 of the δ-force (Sec. VI B), nuclear deformations, the minima of the potential energy surfaces (PES) (Sec. VI C), nuclear masses calculated according to LSD model and the shell correction (Sec. VI D), root mean square radii (Sec. VI E), and quadrupole moments (Sec. VI F) of nuclear charge distributions. Section VII contains the discussion of the results and the hints for further research.

II. HAMILTONIAN

The nucleus is described microscopically as a system of particles which are moving in a deformed mean field and interact through state dependent δ-pairing forces. The Hamiltonian for one type of nucleons reads

$$\hat{H} = \hat{H}_{\rm sp} + \hat{H}_{\rm pair}, \tag{1}$$

where

$$\hat{H}_{\rm sp} = \sum_a \langle a|\hat{h}|a\rangle (c_a^\dagger c_a + c_{\bar{a}}^\dagger c_{\bar{a}}), \tag{2}$$

$$\hat{H}_{\rm pair} = -\sum_{a,b>0} V_{a\bar{a}b\bar{b}} c_a^\dagger c_{\bar{a}}^\dagger c_{\bar{b}} c_b = -\sum_{a,b>0} g_{ab} c_a^\dagger c_{\bar{a}}^\dagger c_{\bar{b}} c_b, \tag{3}$$

where $|a\rangle$ is a single particle state, $|\bar{a}\rangle$ is its time reversed partner, $V_{a\bar{a}b\bar{b}}$ is a pairing matrix element (see Sec. III), and the summation runs only over the single particle states. We use the single particle Hamiltonian

$$\hat{h} = -\frac{\hbar^2}{2m}\Delta + v + v_{ls} + v_{l^2} \tag{4}$$

where the potential part v reads

$$v = \tfrac{1}{2} m[\omega_\perp (x^2 + y^2) + \omega_z z^2], \tag{5}$$

and the oscillator frequencies are parametrized according to Ref. [2]. The shell (N) dependent parameters of $\boldsymbol{l}\cdot\boldsymbol{s}$ and l^2 terms are given as in Ref. [32]

$$v_{ls} = -2\hbar\omega_0 \kappa_{Nl} \boldsymbol{l}\cdot\boldsymbol{s}, \tag{6}$$

$$v_{l^2} = -\hbar\omega_0(\mu_{Nl} l^2 - \langle \mu_{Nl} \boldsymbol{l}^2\rangle_N), \tag{7}$$

where

$$\kappa_{Nl} = \kappa_0[1 + 8\mu_{Nl}(N + 3/2)] + \kappa_1 P_{s,Nl}, \tag{8}$$

$$\mu_{Nl} = \mu_0 P_{k,Nl} \tag{9}$$

and $P_{s,Nl}, P_{k,Nl}$ are the integrals defined by

$$P_{s,Nl} = A^{1/3} \int_0^{R_0 - a/2} R_{Nl}^2(r) r^2 \, dr, \tag{10}$$

$$P_{k,Nl} = \int_{R_0 - a/2}^{R_0 + a/2} R_{Nl}^2(r) r^2 \, dr. \tag{11}$$

In the formulas above R_0 is the nuclear radius: $R_0 = r_0 A^{1/3}$, a stands for the average surface diffuseness of the nuclear density, and A is the mass number. For the rare earth region of nuclei considered in the present paper we take $A=165$, $r_0 = 1.2$ fm, and $a = 0.7$ fm. Other parameters are equal to those of Ref. [32]: $\kappa_0 = 0.021$, $\kappa_1 = 0.9$, and $\mu_0 = 0.062$.

In case of $\kappa_1 = 0$ and $\mu_{Nl} = \mu$, the $\hat{h}$ Hamiltonian reduces to the ordinary Nilsson Hamiltonian [2].

The potential part of the single particle Hamiltonian [Eq. (4)] in stretched coordinates ξ, η, ζ, where $\xi = x\sqrt{M\omega_\perp/\hbar}$, etc., reads

$$v_{/osc} \tfrac{1}{2}\rho^2 \hbar\omega_0 \left[1 - \tfrac{2}{3} P_2(\cos\,\theta)\right], \tag{12}$$

and is replaced by the potential including the higher multipolarities as in Refs. [2,33]

$$v_{\rm osc} = \frac{1}{2}\rho^2\hbar\omega_0 \left[1 - \frac{2}{3}P_2(\cos\,\theta) + 2\sum_{l=4,6} P_l(\cos\,\theta)\right]. \tag{13}$$

The same single particle Hamiltonian was used in Refs. [6,7] to calculate the nuclear radii in case of monopole pairing force with constant matrix element $V_{a\bar{a}b\bar{b}} = G$.

III. δ-PAIRING FORCE

A schematic pairing Hamiltonian is defined using constant pairing matrix element G depending on the size of energy window in which the pairing is present. Constant G is usually adjusted depending on atomic mass region. This kind of pairing forces leads to many fruitful results. However, in treating fission process or the nuclei far from stability for which the pairing strength cannot be determined (no experimentally known masses or gap parameters) the method is only a questionable extrapolation. It is more convenient in such situations to use the state dependent pairing with two strength parameters (one for protons and one for neutrons), possibly the same for the whole periodic table. The state

dependent pairing of the δ-type [15] or Gogny-type interaction [34,35] serve as good candidates for such an approach. In this section we are considering the δ-type pairing interaction.

The Nilsson state $\Phi_a \equiv |a\rangle$ can be cast in the form

$$\Phi_a = \sum_{\{\alpha\},\Sigma=\pm 1/2} C_a^{\alpha,\sigma_\Sigma} |\alpha_a^{\sigma_\Sigma}\rangle |\Sigma\rangle, \tag{14}$$

where α denotes the quantum numbers of the basis states but the third component of spin $\Sigma = \pm 1/2$ and σ_Σ denotes the sign of Σ. Equation (14) can be rewritten as follows:

$$\begin{aligned}\Phi_a &= \sum_{\{\alpha\}} C_a^{\alpha,+} |\alpha_a^{+}\rangle \left|+\tfrac{1}{2}\right\rangle + \sum_{\{\alpha\}} C_a^{\alpha,-} |\alpha_a^{-}\rangle \left|-\tfrac{1}{2}\right\rangle \\ &= \Phi_{a,+} |+\rangle + \Phi_{a,-} |-\rangle, \end{aligned} \tag{15}$$

where $\Phi_{a,\pm}$ are the spin up (+) and spin down (−) components of Φ_a,

$$\Phi_{a,\pm} = \sum_{\{\alpha\}} C_a^{\alpha,\pm} |\alpha_a^{\pm}\rangle. \tag{16}$$

The spinor form of Φ_a allows for easy calculations of matrix elements of the pairing interaction which depends on spin matrices $\boldsymbol{\sigma}$ see Eq. (20). The antisymmetrized matrix element $V_{a\bar{a}b\bar{b}}$ entering the pairing Hamiltonian (3) is given by

$$\begin{aligned} V_{a\bar{a}b\bar{b}} = \int d^3r_1\, d^3r_2\, \Phi_a^\dagger(\vec{r}_1)\, \Phi_{\bar{a}}^\dagger(\vec{r}_2)\, V^\tau(\vec{r}_1, \boldsymbol{\sigma}_1; \vec{r}_2, \boldsymbol{\sigma}_2) \\ \times [\Phi_b(\vec{r}_1)\, \Phi_{\bar{b}}(\vec{r}_2) - \Phi_{\bar{b}}(\vec{r}_1)\, \Phi_b(\vec{r}_2)], \end{aligned} \tag{17}$$

where $\Phi^\dagger$ is Hermite conjugate of Φ and the time reversal spinor $\Phi_{\bar{a}}$ is defined by [36]

$$\Phi_{\bar{a}} = -iK\boldsymbol{\sigma}_y \Phi_a\ , \tag{18}$$

and K is the complex conjugation operator. For the spin up/down components $\Phi_{a,\sigma}|\sigma\rangle$, where $\sigma = \pm$, one has

$$\Phi_{\bar{a},\sigma} = -2\sigma \Phi_{a,-\sigma}^*. \tag{19}$$

The interaction $V^\tau(\vec{r}_1, \boldsymbol{\sigma}_1; \vec{r}_2, \boldsymbol{\sigma}_2)$ is the pairing force of δ-type introduced in Ref. [15]

$$V^\tau(\vec{r}_1, \boldsymbol{\sigma}_1; \vec{r}_2, \boldsymbol{\sigma}_2) = V_0^\tau \frac{1 - \boldsymbol{\sigma}_1 \cdot \boldsymbol{\sigma}_2}{4} \delta(\vec{r}_1 - \vec{r}_2). \tag{20}$$

While

$$\boldsymbol{\sigma}_1 \cdot \boldsymbol{\sigma}_2 = \begin{cases} 1 \text{ for } S = 1 \\ -3 \text{ for } S = 0, \end{cases} \tag{21}$$

one has

$$\frac{1 - \boldsymbol{\sigma}_1 \cdot \boldsymbol{\sigma}_2}{4} = \begin{cases} 0 \text{ for } S = 1 \\ 1 \text{ for } S = 0. \end{cases} \tag{22}$$

We consider here the case of $T=1$ pairing, i.e., the p-p and n-n pairing only. Taking this into account one obtains

TABLE I. The parameters of the LSD model [27] appearing in Eq. (26).

Term	Units	LSD
$b_{\rm vol}$	MeV	−15.4920
$\kappa_{\rm vol}$		1.8601
$b_{\rm surf}$	MeV	16.9707
$\kappa_{\rm surf}$		2.2938
$b_{\rm cur}$	MeV	3.8602
$\kappa_{\rm cur}$		−2.3764
r_0	fm	1.21725
C_4	MeV	0.9181

$$\begin{aligned} V_{a\bar{a}b\bar{b}} &= \int d^3r [\Phi_{a,+}^* \Phi_{a,+} \Phi_{b,+}^* \Phi_{b,+} + \Phi_{a,-}^* \Phi_{a,-} \Phi_{b,-}^* \Phi_{b,-} \\ &\quad + \Phi_{a,+}^* \Phi_{a,+} \Phi_{b,-}^* \Phi_{b,-} + \Phi_{a,-}^* \Phi_{a,-} \Phi_{b,+}^* \Phi_{b,+}] \\ &= \int d^3r \sum_{s,s'=\pm} |\Phi_{a,s}|^2 |\Phi_{b,s'}|^2. \end{aligned} \tag{23}$$

The pairing gap equations become

$$\Delta_a = \frac{1}{2} \sum V_{a\bar{a}b\bar{b}} \frac{\Delta_b}{\sqrt{(\epsilon_b - \lambda)^2 + \Delta_b^2}}. \tag{24}$$

The occupation probabilities are given by

$$v_a^2 = \frac{1}{2}\left(1 - \frac{\epsilon_a - \lambda}{\sqrt{(\epsilon_a - \lambda)^2 + \Delta_a^2}}\right). \tag{25}$$

IV. NUCLEAR MASSES AND LSD MODEL

There has been recently an impressive increase of the accuracy of measurements of nuclear masses. The Penning trap measurement leads to accuracy of about 10 keV (see, e.g., Ref. [37]). There is also an increase in the number of nuclei far from β stability for which the mass has been recently measured and this is expected to be continued, due to the fast progress in the development of techniques of radioactive ion beams (e.g., Ref. [8]).

It was shown [27] that the liquid drop model which in addition to the volume, surface, and Coulomb terms contains only the first order curvature term satisfactorily describes the nuclear binding energies. The parameters of the LSD model were found by fitting the LSD masses to 2766 experimental masses of Ref. [38]. The parameters are listed in Table I. The mean square deviation of the binding energies of the model equals to $\delta M = 0.698$ MeV.

The nuclear mass according to the curvature dependent LSD model [27] is given by the formula

$$\begin{aligned} M(Z,N;\text{def}) &= ZM_{\rm H} + NM_{\rm n} - 0.000\,014\,33\, Z^{2.39} \\ &\quad + b_{\rm vol}\ (1 - \kappa_{\rm vol} I^2)\, A + b_{\rm surf}\, (1 - \kappa_{\rm surf} I^2) \\ &\quad \times A^{2/3} B_{\rm surf}(\text{def}) + b_{\rm cur}\ (1 - \kappa_{\rm cur} I^2) \end{aligned}$$

$$\times A^{1/3} B_{\mathrm{cur}}(\mathrm{def}) + \frac{3}{5}\, e^2 \frac{Z^2}{r_0^{ch} A^{1/3}}\, B_{\mathrm{Coul}}(\mathrm{def})$$

$$- C_4 \frac{Z^2}{A} + E_{\mathrm{micr}}(Z, N; \mathrm{def}) + E_{\mathrm{cong}}(Z, N),$$

where

$$E_{\mathrm{micro}} = E_{\mathrm{pair}} + E_{\mathrm{shell}}, \tag{27}$$

$$E_{\mathrm{cong}} = -(10\ \mathrm{MeV}) \exp(-42|I|/10). \tag{28}$$

B_x are the coefficients which depend on the geometry of the nuclear shape and are defined as the ratio of the corresponding energies of the deformed and the spherical nucleus

$$B_x = \frac{E_x(\mathrm{def} \neq 0)}{E_x(\mathrm{def} = 0)}. \tag{29}$$

The definitions of the curvature B_{cur}, Coulomb B_{Coul}, and surface B_{surf} coefficients remain the same as in the drop model (Coulomb and surface coefficients) or in droplet model (curvature coefficient B_{cur}) [28,29].

V. NUCLEAR RADII

Progress in measuring nuclear radii is also large (see, e.g., Refs. [39–41]). All this is a challenge for the theory. The theoretical calculations of the rms charge radii are very common in different theoretical frameworks (see, e.g., Refs. [7,26,42], and the references cited therein).

The rms radius $\langle r^2 \rangle$ of the distribution of the point-like protons is calculated as the expectation values of r^2 in the BCS ground state of the system

$$\langle r^2 \rangle = \langle \mathrm{BCS}|r^2|\mathrm{BCS}\rangle = \sum_{k>0} 2v_k^2 \langle k|r^2|k\rangle. \tag{30}$$

The finite proton size and its internal charge distribution are taken into account through the formula

$$r_{\mathrm{ch}}^2 = \langle r^2 \rangle + s_p^2, \tag{31}$$

where r_{ch} is the rms charge radius corresponding to the finite proton size and $s_p = 0.8$ fm [43] is the rms charge radius inside the finite proton alone.

VI. RESULTS

Extended numerical calculations have been performed for the set of nuclei from the rare earth region [Z=58(2)72] for which the pairing gaps were possible to be calculated from experimental masses. The results are divided into a few parts. First we discuss in detail the δ-pairing matrix elements and the corresponding gap parameters in Sec. VI A. In the following section the state dependent δ-pairing strength constants V_0 are adjusted for both protons and neutrons. Then the calculations of nuclear radii, masses, and quadrupole moments are performed with the fixed values of strength constants and their presentation is done in the following sections.

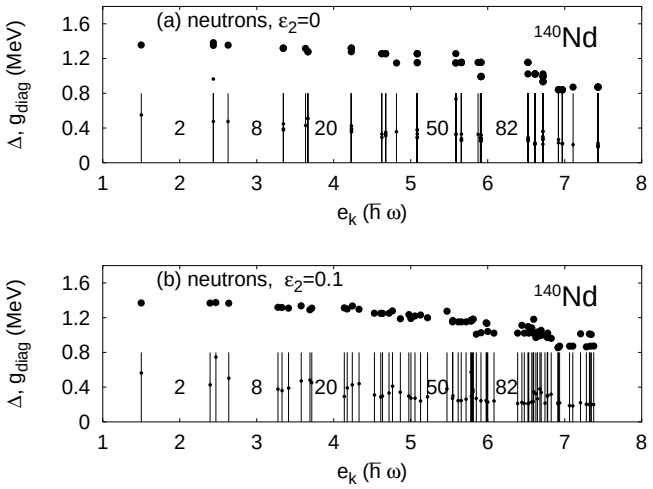

FIG. 1. Gap parameter Δ (big filled circles) and diagonal antisymmetrized matrix elements $g_{\mathrm{diag}}=g_{aa}=(a\bar{a}|V_\delta|a\bar{a})$ (small filled circles) in MeV vs single particle energies (in units of $\hbar\omega$) for neutrons in ^{140}Nd nucleus. Part (a) corresponds to spherical case $\epsilon_2=\epsilon_4=\epsilon_6=0$ while (b) corresponds to the deformation $\epsilon_2=0.1$. The vertical lines represent the single particle spectrum. The magic neutron numbers are also shown. In the spherical case the gaps for degenerate levels are nearly equal. In case (b) corresponding to a slightly deformed nucleus, the degeneracy of levels is removed and a very weak dependence of Δ_a gaps on single particle energies is observed. The strengths V_0 used in calculations are given in Table III.

A. δ-pairing matrix elements and gap parameters

In the following section the matrix elements g_{ab} [see Eqs. (3) and (17)] and the gap parameters Δ for the representative case of nearly spherical nucleus ^{140}Nd are discussed and displayed in figures separately for protons and neutrons. The values of V_0 used in calculations of pairing gaps Δ_a correspond to the values given in Sec. VI B (see Table III).

The ground state deformations have been calculated by many groups of authors but the results of the state dependent version of BCS approach are nearly absent in the publications. Thus it seems to be worth and interesting to look here at the calculated values of the δ-pairing matrix elements $g_{ab}=(a\bar{a}|V_\delta|b\bar{b})$ and the BCS derived values of the gap parameters Δ_a as a function of the single particle energies and/or number of particles as well as their dependence on the nuclear shape deformation. The dependencies of this kind are shown in the following figures (Figs. 1–5).

Figure 1 shows the gap parameter Δ (big filled circles) as well as diagonal antisymmetrized matrix elements of the state dependent δ-pairing interaction $g_{\mathrm{diag}}=g_{aa}=(a\bar{a}|V_\delta|a\bar{a})$ (small filled circles) in MeV vs single particle energies. The single particle energies are in units of $\hbar\omega$. The figure is for neutrons in a nearly magic ^{140}Nd nucleus. Part (a) of the figure corresponds to the spherical case $\epsilon_2=\epsilon_4=\epsilon_6=0$ while its second part (b) is for the deformation $\epsilon_2=0.1$. The vertical lines represent the single particle spectrum of the nucleus ^{140}Nd. The magic neutron numbers corresponding to the closed shells are also displayed. In case of spherical nucleus (a), the gaps Δ_a for the degenerate levels show a small de-

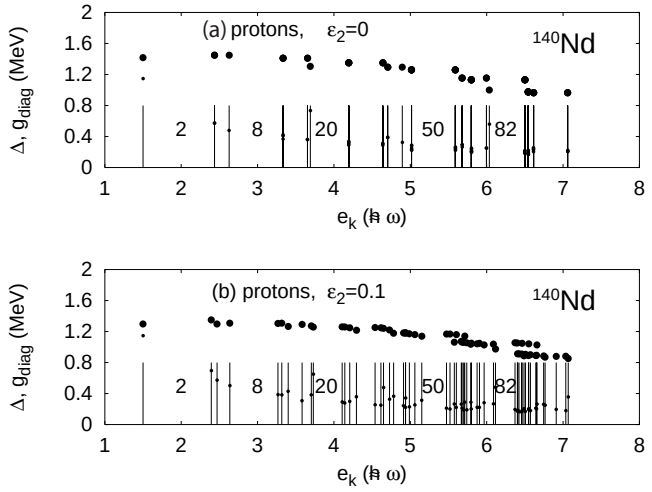

FIG. 2. Same as in Fig. 1 but for protons.

crease with increasing energy. The maximal value of $\Delta_a \approx 1$ MeV corresponds to the lowest magic shell (N=2) and decreases down to the value of 0.7 MeV in case of the single particle levels above N=82.

Case (b) of Fig. 1 corresponds to slightly deformed nucleus at deformation ϵ=0.1. The single particle levels are already not degenerate and one observes a small spread of values of Δ_a for each shell. There is also a dependence of Δ_a gaps on the single particle energies along the whole single particle spectrum. The global decrease of Δ_a vs energy is comparable to that for the spherical case. However, the values of Δ_a for the deformed case are lower on about 0.15 MeV as compared to the spherical case.

Closer look at Figs. 1 and 2 shows that there are only few different values of Δ_a inside each degenerate shell (at ϵ_2=0). The degeneracy of gap parameter Δ_a is removed already at small deformations and one observes the spreading of Δ_a values for $\epsilon_2 > 0$. In terms of single particle Nilsson levels it

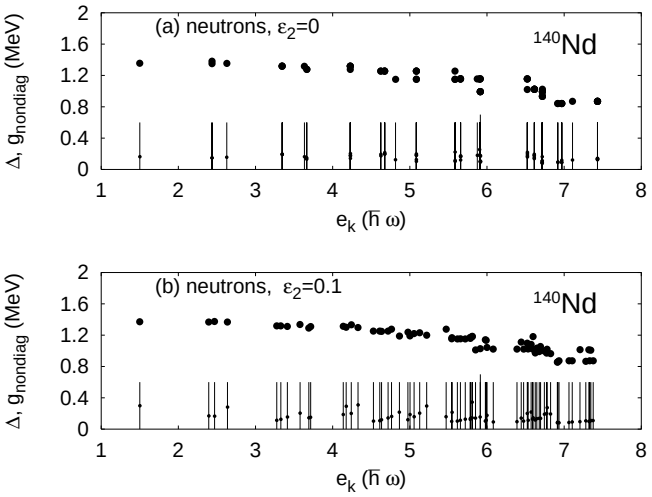

FIG. 3. Same as in Fig. 1 but for nondiagonal matrix elements $g_{\rm nondiag}=g_{a\rm F}=(a\bar{a}|V_\delta|F\bar{F})$ which couple to the Fermi level F. The energy of the Fermi level is shown as a longer and thicker vertical line in the single particle spectrum.

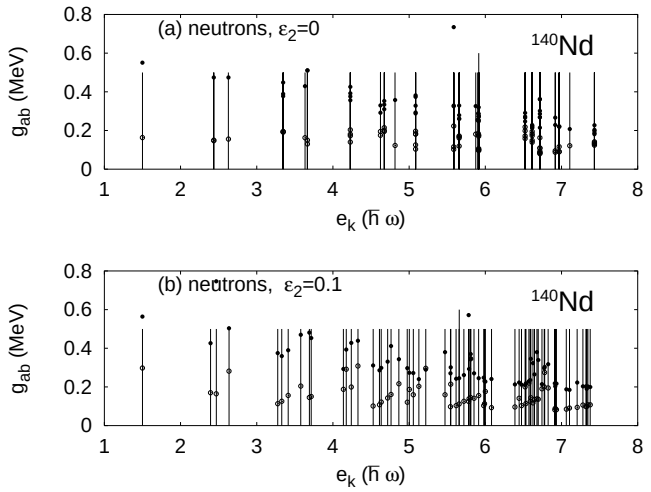

FIG. 4. Diagonal $g_{\rm diag}=g_{aa}=(a\bar{a}|V_\delta|a\bar{a})$ (filled circles) and nondiagonal $g_{a\rm F}=(a\bar{a}|V_\delta|F\bar{F})$ coupled to Fermi level F matrix elements of the δ-pairing interaction vs single particle energies (MeV) for two different deformations in ^{140}Nd. Part (a) corresponds to ϵ_2=0 and part (b) to ϵ_2=0.1.

corresponds to the fact that a single particle state $|a\rangle$ is an admixture of different j shells (j-basis states), e.g.,

$$|a\rangle = |N\ \Omega\ \nu\rangle = \sum_j\ C^{N\ \Omega\ \nu}_{l\ j}|N\ l\ j\ \Omega\rangle, \tag{32}$$

where ν stands for other q numbers. For small deformations, in the set of expansion coefficients $C^{N\ \Omega\ \nu}_{l\ j}$ still dominates a "main shell" j value causing rather small spread of Δ_a values that is illustrated in Table II. The table shows the largest *diagonal* contributions of the basis states $|Nlj\Omega\rangle$ to the δ-pairing force matrix element $g_{N\Omega,N\Omega}$ (in spherical oscillator basis $|Nlj\Omega\rangle$) for V_0=240 MeV fm^{-3} for protons in ^{154}Nd. We select at random two typical wave functions $|N\Omega\rangle=|3,5/2\rangle$ and $|N\Omega\rangle=|3,1/2\rangle$ with energies $\epsilon_{N=3\ \Omega=5/2}=4.149\hbar\omega$ and $\epsilon_{N=3\ \Omega=1/2}=4.599\hbar\omega$ at spherical configuration. The increase of deformation leads to the state

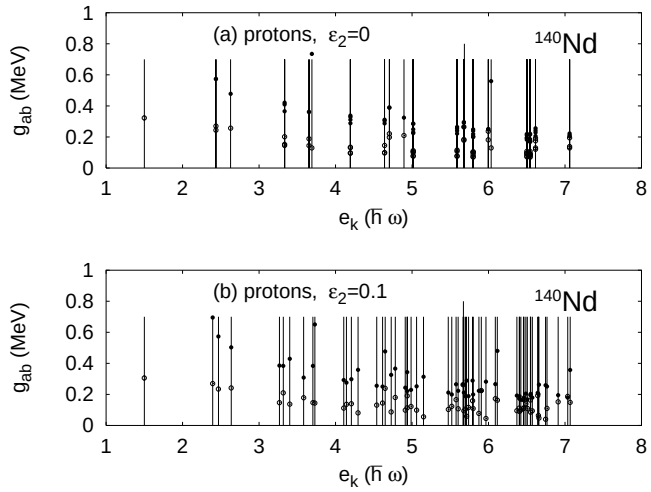

FIG. 5. Same as in Fig. 4 but for protons.

TABLE II. The *diagonal* contributions $g_{Nlj\Omega,Nlj\Omega}$ of spherical basis states $|Nlj\Omega\rangle$ to the δ-pairing matrix elements $g_{N\Omega,N\Omega}$ for protons in ^{154}Nd. Two states from the main shell $N=3$ are shown. In the second column the energy of the Nilsson model state $|N\Omega\rangle$ in $\hbar\omega$ units is given. Third column gives the squared coefficient $C_{lj}^{N\Omega}$ in the expansion $|N\Omega\rangle=\Sigma_{lj}\ C_{lj}^{N\Omega}|N\Omega lj\rangle$ and the following one shows the quantum numbers $|Nlj\Omega\rangle$ of the base states. The contributions $g_{Nlj\Omega,Nlj\Omega}$ of the state $|Nlj\Omega\rangle$ to the matrix element $g_{N\Omega,N\Omega}$ are given in column five. The last column gives the total value of $g_{N\Omega,N\Omega}$ in the state $|N\Omega\rangle$. Parts (i), (ii), and (iii) of the table correspond to the deformations $\epsilon_2=0$, 0.2, and 0.4, respectively ($V_0=240$ MeV fm^{-3}).

$\|N\ \Omega\rangle$	$e_{N\Omega}(\hbar\omega)$	$\|C_{l\ j}^{N\Omega}\|^2$	$\|N\ l\ j\ \Omega\rangle$	$g_{Nlj\Omega,Nlj\Omega}$	$g_{N\Omega,N\Omega}$
(i) $\epsilon_2=0$					
$\|3\ 5/2\rangle$	4.149	1.0000	$\|3\ 3\ 7/2\ 5/2\rangle$	0.0976	0.2254
$\|3\ 1/2\rangle$	4.599	1.0000	$\|3\ 1\ 3/2\ 1/2\rangle$	0.2219	0.3328
(ii) $\epsilon_2=0.2$					
$\|3\ 5/2\rangle$	4.192	0.9919	$\|3\ 3\ 7/2\ 5/2\rangle$	0.0960	0.2254
$\|3\ 1/2\rangle$	4.451	0.4871	$\|3\ 1\ 3/2\ 1/2\rangle$	0.0526	0.2247
		0.1033	$\|3\ 3\ 7/2\ 1/2\rangle$	0.0010	
		0.2068	$\|3\ 3\ 5/2\ 1/2\rangle$	0.0042	
		0.2028	$\|3\ 1\ 1/2\ 1/2\rangle$	0.0091	
(iii) $\epsilon_2=0.4$					
$\|3\ 5/2\rangle$	4.276	0.9776	$\|3\ 3\ 7/2\ 5/2\rangle$	0.0932	0.2254
		0.0224	$\|3\ 3\ 5/2\ 5/2\rangle$	0.0001	
$\|3\ 1/2\rangle$	4.291	0.2666	$\|3\ 1\ 1/2\ 1/2\rangle$	0.0158	0.1949
		0.2090	$\|3\ 3\ 7/2\ 1/2\rangle$	0.0043	
		0.3989	$\|3\ 3\ 5/2\ 1/2\rangle$	0.0155	
		0.1255	$\|3\ 1\ 3/2\ 1/2\rangle$	0.0035	

mixture (measured by the values of the expansion coefficients $C_{lj}^{N\Omega}$ shown in column 3) of the basis states and to the decrease of the main shell state contribution $g_{Nlj\Omega\ Nlj\Omega}$ (columns 4 and 5). This behavior is typical for all of the matrix elements.

The dependence in energy of Δ_a follows that of the diagonal matrix elements g_{aa} on the energy. This matrix elements are shown in the same figure (see Figs. 4 and 5 for more details and explanation). Gap parameters for neutrons and protons behave very similarly what is illustrated in Fig. 2.

Figures 4 and 5 show values of the diagonal as well as nondiagonal matrix elements g_{ab} for neutrons and protons, respectively, in ^{140}Nd. The matrix elements connecting a state whose energy is closest to the Fermi energy with any other state are shown. Filled circles correspond to diagonal g_{aa} values while the open circles are the values of g_{aF}. The Fermi level is shown also in the plot as a longer and thicker vertical line. One observes here a few interesting features.

(i) The values of the diagonal matrix elements are larger than nondiagonal ones about a factor of 1.5–2 on an average.

(ii) The nondiagonal matrix elements g_{aF} are rather "randomly" distributed around some average value; no long range energy dependence is observed.

(iii) The diagonal matrix elements g_{aa} show the regular decrease of the average value with the increase of the single particle energy.

(iv) There is always a dominant matrix element g_{aa} inside each shell which is on a factor of 1.5–2 larger than the smallest matrix element present in the shell.

(v) The average $\overline{g_{aa}}$ linearly decreases with increasing energy.

(vi) The average dependence of $\overline{g_{aa}}$ on particle number $2n$ filling the levels up to the considered level a behaves like a function const$/(2n)^{2/3}$, where the proportionality constant is close to 3 MeV. A similar behavior of the constant matrix element G was already observed [44] and is a characteristic feature of the spectra build on the basis of harmonic oscillator potentials. All the properties discussed so far apply for larger nuclear deformations.

B. Pairing strength V_0

Both the strength V_0 and the energy width of the pairing window are connected through the condition of the equality of experimental energy gap parameter Δ and the gap determined from the BCS equations (24) for the Fermi level. A variety of energy cutoff procedures is used (see, e.g., Refs. [20,45,46]). All of them give the values of the pairing strength depending on the energy cutoff or on the number of levels in the pairing window.

There are also different types of approximations for the experimental gaps $\Delta_{\rm exp}$. Different approaches use various numbers of experimental masses in the gap formula [43,47]. The very modern view on this problem is presented in an approach which was undertaken in Ref. [48], where the new formula for the "*pairing indicator* $\Delta^{(3)}$ was derived. It involves three experimental masses and is proved to be a proper estimate of the pairing gap parameter. $\Delta^{(3)}$ differs significantly from the gaps calculated so far. The gap is defined as [48] [Eq.(1)]

$$\Delta^{(3)}(N)=\frac{\pi_N}{2}[B(N-1)+B(N+1)-2B(N)], \qquad (33)$$

where $\pi_N=(-1)^N$ is the parity of N number and $B(N)$ is the binding energy of the system consisting of N particles.

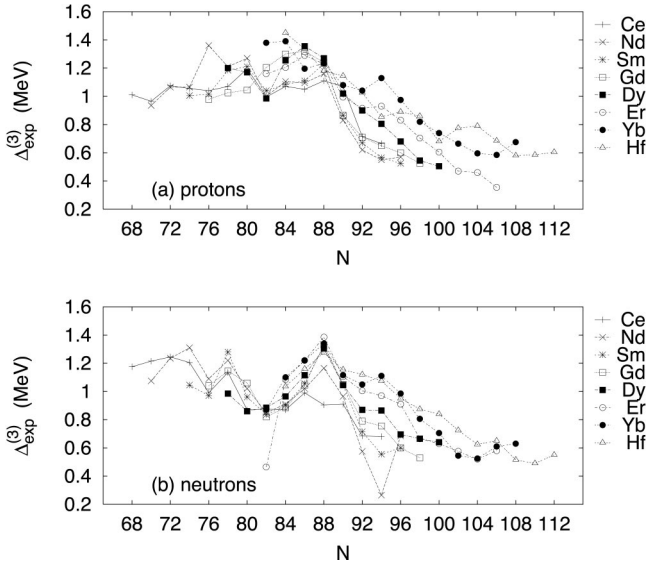

FIG. 6. The experimental pairing indicator $\Delta^{(3)}_{\rm exp}$ for rare earth nuclei. Part (a) of the figure is for protons and part (b) for neutrons.

The quality of $\Delta^{(3)}$ is also discussed [46]. In the present paper we follow the definition of the gap parameter as given by Eq. (33).

The formula for the average behavior of $\Delta^{(3)}(A)$ as a function of the mass number A does not match the well known $12/\sqrt{A}$ dependence (see Ref. [43]). The $\Delta^{(3)}$ pairing indicators for rare earth nuclei are shown in Fig. 6. In part (a) of the figure one sees $\Delta^{n}_{\rm exp}$ of neutrons and in part (b) $\Delta^{p}_{\rm exp}$ of protons. The average behavior of $\Delta_{\rm exp}$ is given by the simple formula

$$\overline{\Delta} = d_{n,p}/N^{1/3}, \tag{34}$$

for both types of nucleons. Here $d_{n,p}$ are constants which differ rather little for both types of nucleons and we have assumed here one value for both kinds of particles

$$d_{n,p} = 5,$$

and N is the number of neutrons or protons.

Integrals (17) were calculated in the Nilsson or Nilsson-Seo Hamiltonian eigenstates directly using the Gauss-Hermite and Gauss-Laguerre integration quadratures [49].

The adjustment of the δ-pairing strength V_0 has to be performed at the energy minimum of the nucleus which is unknown initially. In order to simplify the procedure of adjusting the strength V_0 of the pairing interaction [see Eq. (20)] we proceed as follows. Our reference point was the results of Ref. [33]. First the grids in the three-dimensional deformation space of $(\epsilon_2, \epsilon_4, \epsilon_6)$ were chosen. We have done this according to the minima of the PES given in Ref. [33]. The grid is defined as

$$\epsilon_2 = \epsilon_{2,m} - 0.06\ (0.04)\ \epsilon_{4,m} + 0.06, \tag{35}$$

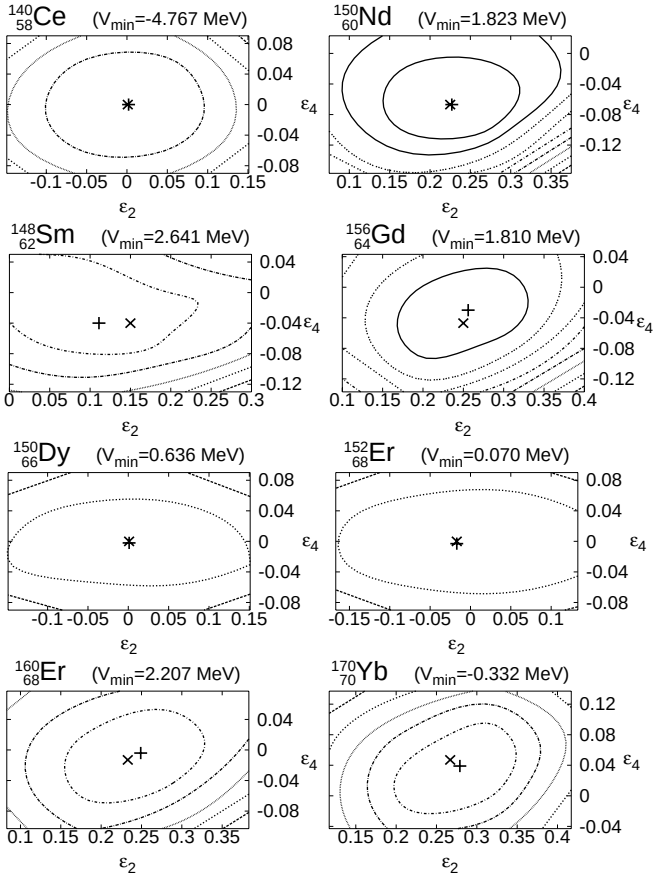

FIG. 7. Potential energy surfaces for some rare earth nuclei. The separation of contour levels equals 2 MeV. The minima of PES are shown by plus sign (+). For comparison the minima calculated in Ref. [33] (times sign, $\times$) are shown.

$$\epsilon_4 = \epsilon_{4,m} - 0.06\ (0.04)\ \epsilon_{4,m} + 0.06, \tag{36}$$

where the subscripts m denote the initial deformation which we took from Ref. [33]. For each nucleus the PES was calculated and the minimum of the total energy was found. The procedure was repeated until the difference of the successive ground state deformations was reasonably small.

The ϵ_6 deformation was treated in a static way, i.e., it was kept equal to $\epsilon_{6,m}$ as in Ref. [33]. This is reasonable while the minimization of PES in three-dimensional space leads to the values of $\epsilon_{6,m}$ nearly equal to the deformations in Ref. [33].

The typical PES are shown in Fig. 7 where the plus sign (+) denotes the minima taken from Ref. [33] and the *times* sign ($\times$) the minima of the PES as calculated here.

The number of levels n in the pairing window is the same as in Ref. [2], i.e., we have assumed $n=2\sqrt{15N(Z)}$.

The adjustment of V_0 can be formulated as a problem of solving the equation

$$\Delta^{n,p}_{\rm exp} = \Delta^{n,p}_{\rm Fermi}(V^{n,p}_0), \tag{37}$$

at the minimum of the total energy of the nucleus, where $\Delta^{n,p}_{\rm Fermi}(V^{n,p}_0)$ corresponds to the Fermi level of neutrons (n) and protons (p), respectively. The procedure involves the

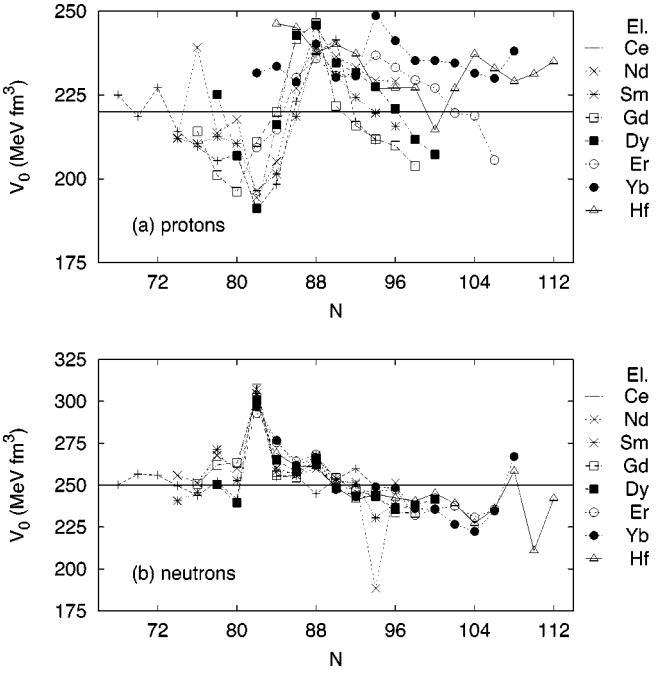

FIG. 8. The strength V_0 of the pairing force in case of Nilsson model as a function of the neutron number N for protons [part (a) of the figure] and for neutrons [part (b) of the figure] for rare earth nuclei. The same isotopes are connected by lines. The average values of V_0 are shown as straight lines.

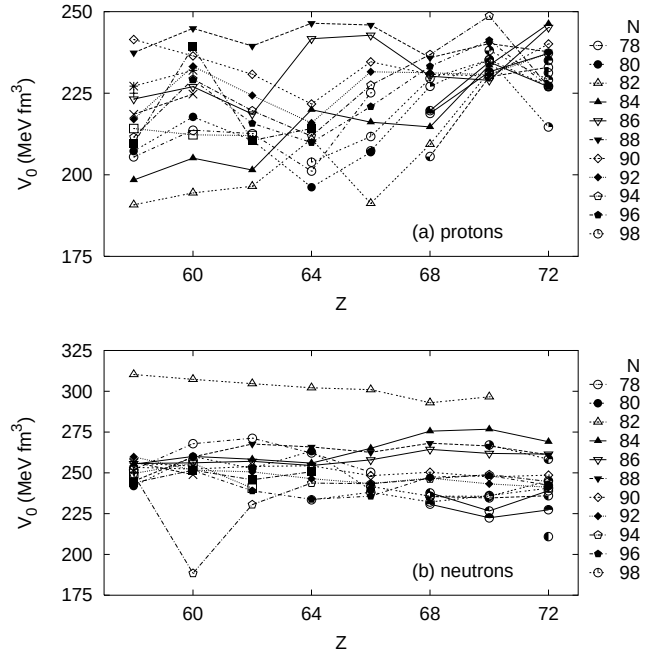

FIG. 9. The strength V_0 of the pairing force in case of Nilsson model as a function of the atomic number Z for protons [part (a) of the figure] and for neutrons [part (b) of the figure] for rare earth nuclei. The same isotones are connected by straight lines. On the right side neutron numbers corresponding to given curves are shown.

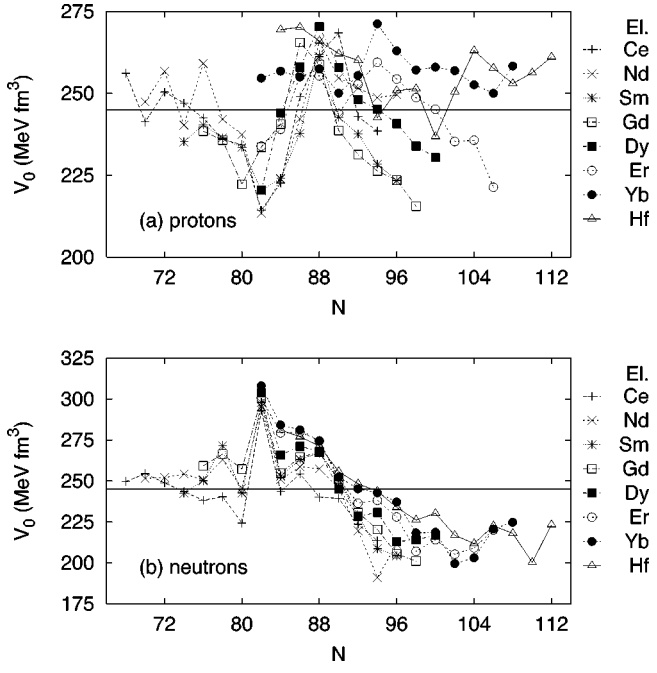

FIG. 10. Same as in Fig. 8 but for Nilsson-Seo model.

solution of the system of $2n+1$ BCS equations (24) for the set of Δ_i gaps and the Fermi level λ in the pairing window. We have used a very effective iterative method of solution of the system of equations (24). Given an initial set of Δ gaps on the right hand side of Eq. (24), the left hand side of it determines the new set of solutions and the procedure is repeated until the assumed accuracy is obtained. At accuracy 0.001 MeV one needs usually only a few iterations to reach the convergence. At the same time the Fermi level was determined by the commonly used Newton method.

In Figs. 8 and 9 exact values of $V_0^{n,p}$ are shown for rare earth nuclei obtained with Nilsson model. The average values of the pairing strength are shown as well. The structure of V_0 seems to be too complicated and was not in fact found as a function of the number of protons Z or neutrons N as well as the isospin $I=(N-Z)/A$, which are typically used in such cases. It is observed that the values of V_0 oscillate in a very irregular manner showing the maxima at the magic numbers and the minima in the middle of the shell. The value of the amplitude of the oscillations is rather small (close to 10 MeV fm^3) and it does not change very much the value of the Δ^F gap corresponding to the Fermi level. Changing V_0 to e.g., 10%, produces only a few percentage change of Δ^F.

Any chain of isotopes at Z=const in Fig. 8 and at N =const in Fig. 9 shows an average decrease of V_0 with in-

TABLE III. δ pairing strength parameters $V_0^{n,p}$ for neutrons and protons, respectively, for rare earth nuclei in units MeV fm^3 adjusted for the pairing window with $n=2\sqrt{15N(Z)}$.

Model	V_0^n	V_0^p
Nilsson	250	220
Nilsson-Seo	245	245

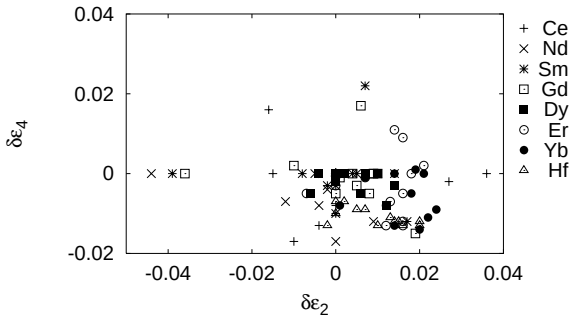

FIG. 11. The differences in the ground state deformations as calculated in the present paper and those given in Ref. [33] for both ϵ_4 and ϵ_2 deformations. Here $\delta\epsilon_4=\epsilon_4-\epsilon_4^m$ and $\delta\epsilon_2=\epsilon_2-\epsilon_2^m$, where superscripts m denote the ground state deformations in Ref. [33] for rare earth nuclei.

creasing neutron number $N=A-Z$ starting at the largest value of V_0 which corresponds to the magic isotopes with well separated energy shells, decreases and then increases again. The latter behavior is observed on the left hand side of the peak of V_0 for the lighter isotopes considered here, i.e., Ce to Er inclusively. There is no net increase or decrease of V_0 in the shell or it is very small. Therefore, it is hard to adopt some simple physically explained dependence.

In consequence, we do not find some typical dependence of V_0 on N, Z, or I. Instead we have assumed the average value of V_0 as the strength of the pairing force for the considered region of nuclei (Fig. 10).

In Table III we show the strength V_0 as adjusted for the rare earth nuclei.

C. Nuclear deformations

Figure 11 shows new equilibrium deformations for the rare earth region. As already said ϵ_6 is the same as in Ref. [33]. In Fig. 12 ϵ_6 vs ϵ_4 is shown. The average ϵ_6 deformation region can be approximated by

$$\epsilon_6 = -0.3\epsilon_4. \tag{38}$$

The boundaries of ϵ_6 deformation are

$$\epsilon_6 = -0.3\epsilon_4 - 0.02, \tag{39}$$

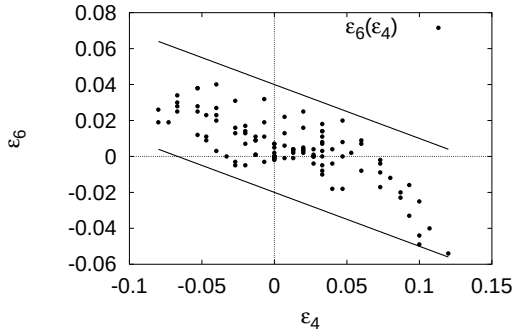

FIG. 12. The deformations ϵ_6 vs ϵ_4 for rare earth nuclei [33].

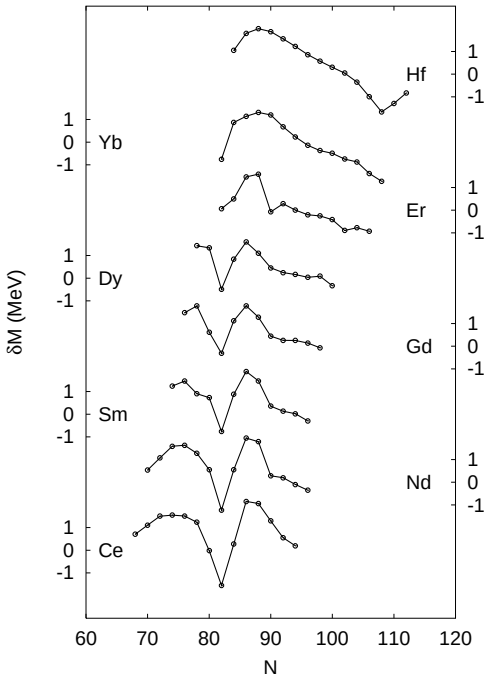

FIG. 13. Same as in Fig. 14 but for Nilsson-Seo potential.

$$\epsilon_6 = -0.3\epsilon_4 + 0.02. \tag{40}$$

This allows for the approximate calculations of PES.

The equilibrium deformations obtained in Ref. [33] and those presented here differ and the difference can be measured by the following rms deviations for ϵ_2 and ϵ_4 deformations, respectively,

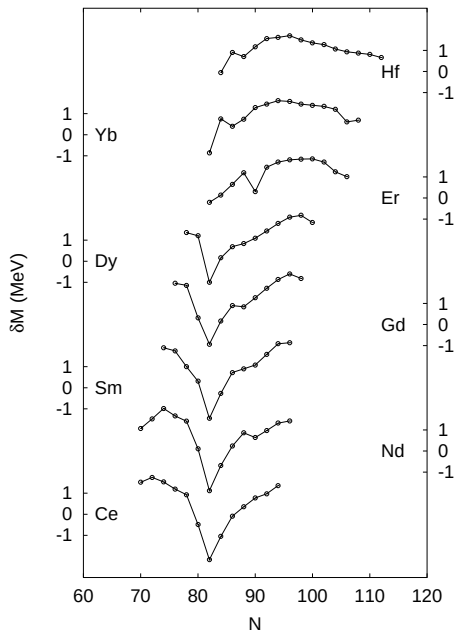

FIG. 14. The mass deviation $\delta M=M_{\rm th}-M_{\rm exp}$ for rare earth nuclei as calculated with the Nilsson model. The experimental data $M_{\rm exp}$ were taken from Audi and Wapstra mass tables [51].

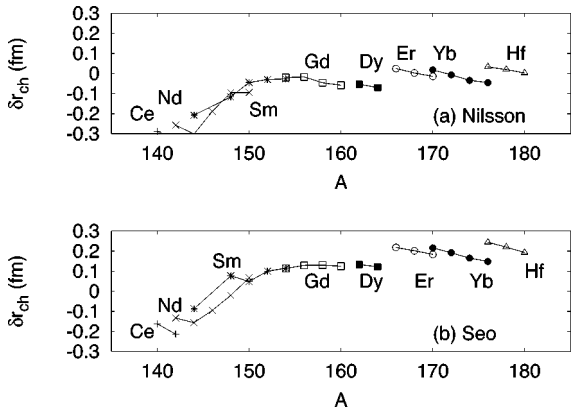

FIG. 15. The charge radius deviation $\delta r_{ch}=r_{\mathrm{ch,th}}-r_{\mathrm{ch,exp}}$ for rare earth nuclei calculated with the Nilsson (a) and Nilsson-Seo (b) models. The experimental data r_{exp} were taken from Refs. [39–41].

$$\sigma_2=\left(\frac{\sum_{n=1}^{n=N}(\epsilon_{2,n}-\epsilon_{2,n}^{m})}{N}\right)^{1/2},\quad \sigma_4=\left(\frac{\sum_{n=1}^{n=N}(\epsilon_{4,n}-\epsilon_{4,n}^{m})}{N}\right)^{1/2}, \tag{41}$$

where N is the number of nuclei in calculations and m stands for equilibrium deformations calculated in Ref. [33]. It was shown that for the considered isotopes $\sigma_2=0.034$ and $\sigma_4=0.02$. The deformations ϵ_3 and ϵ_5 were not taken into account while they do not appear in the considered region of nuclei and in case of the minima of PES. The deformations ϵ_6 equals in both Ref. [33] and our case.

While the nuclear deformation parameters cannot be directly compared to their experimental equivalents the more distinct comparison of our results concerning the nuclear shapes is presented in Sec. VI F where the quadrupole moments which are the proper observables measuring the nuclear deformations are shown.

D. Nuclear masses

The mass of the nucleus is totally determined by Eq. (26). In the following the mass excess

$$ME=M(Z,N,\mathrm{def})-Z\mathcal{M}_H-N\mathcal{M}_n \tag{42}$$

is calculated and compared to experimental data [50,51]. Here $\mathcal{M}_H$ and $\mathcal{M}_n$ are the mass excesses for hydrogen atom and the neutron, respectively. The results are shown in Fig. 13 for Nilsson-Seo potential and in Fig. 14 for rare earth region for the pure Nilsson model. The rms deviation for *ME* evaluated for all considered nuclei is less than 0.7 MeV in both the considered models. This value of accuracy in determining the nuclear mass is comparable to the corresponding values obtained in more refined theories [26,33]. The comparison of nuclear masses calculated for spherical nuclei in Skyrme+HF, Gogny+HF as well as the RMF model was also presented in Refs. [52–54]. The quality of those estimates of the nuclear masses for a sample of 116 spherically symmetric nuclei is comparable to the present one.

There is a systematic deviation between the two models studied: the masses as calculated using Nilsson approach are better as compared to the version of Nilsson-Seo model. In Seo model there is only one set of potential parameters κ_0, κ_1, and μ_0 which regulate the dependence of the potential on the spin-orbit $\boldsymbol{l}\cdot\boldsymbol{s}$ and the $\boldsymbol{l}^2$ terms [see Eqs. (9). The dependence on atomic number A enters here through the "universal" assumptions made in Eq. (11). The parameters κ_0, κ_1, and μ_0 are common for both protons and neutrons and are the same for the whole periodic table. On the other hand, one has four analogous parameters in the pure Nilsson model and the values of them are different in various nuclear regions for which they are adjusted to reproduce the single particle level spacings characteristic to the region in question. It seems that the universal behavior of the Nilsson-Seo parameters as given in Eq. (11) is too simple and does not mimic the proper A dependence of the parameters. The mass deviations seem to be the consequence of this fact.

E. Charge root mean square radii

The root mean square radii $\langle r^2\rangle$, Eq. (31), are compared to experimental data [39–41] in Fig. 15. It was pointed out in Ref. [7] that the best fit to experimental data is achieved if one assumes the Nilsson oscillator frequency $\hbar\omega_0^0=40/A^{1/3}$ and the standard isospin dependence of $\hbar\omega_0$ is changed for the following one

$$\hbar\omega_0^Z=\frac{40}{A^{1/3}},\quad \hbar\omega_0^N=\frac{40}{A^{1/3}}\left(\frac{N}{Z}\right)^{1/3}, \tag{43}$$

where N and Z are neutron and proton numbers, respectively.

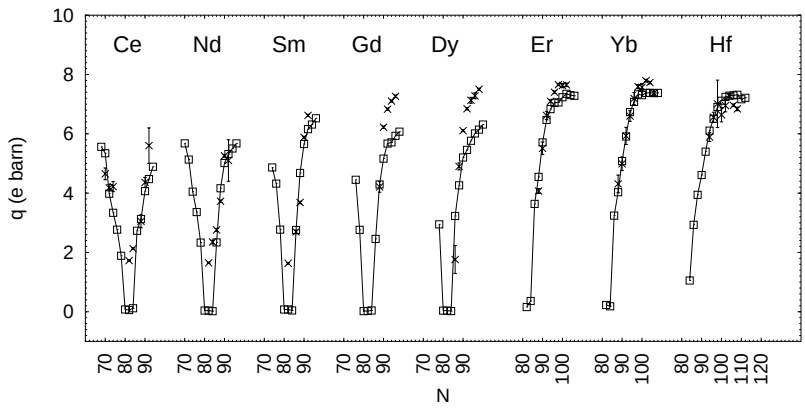

FIG. 16. Quadrupole moments of rare earth nuclei calculated with the Nilsson model (open squares, □) in comparison to experimental data (× with error bars) which were extracted from Refs. [55,56].

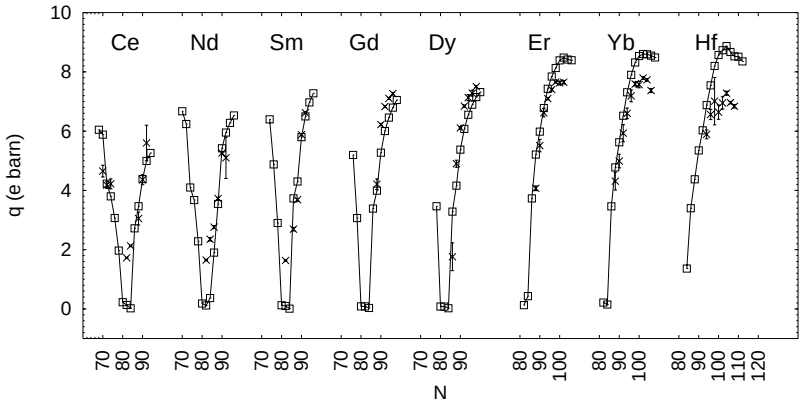

FIG. 17. Same as in Fig. 16 but for Nilsson-Seo model.

In case considered here the constant 40 used in Ref. [7] is too small and we adopt the larger value of it, namely, 41.

Despite of this choice of $\hbar\omega_0^0$ there are large discrepancies between the model calculations and the experimental data especially in case of heavier nuclei.

F. Quadrupole moments

The quadrupole moment Q is calculated as an expectation value of the quadrupole moment operator

$$\hat{Q} = 2P_2(\cos\,\theta) \tag{44}$$

in the proton sector of the BCS ground state of the nucleus. In Eq. (44) $P_2(\cos\,\theta)$ is the Legendre polynomial. This leads to the expression

$$Q = \langle \mathrm{BCS}|\hat{Q}|\mathrm{BCS}\rangle = \sum_{k>0} 2v_k^2\langle k|\hat{Q}|k\rangle, \tag{45}$$

where v_k^2 are the occupation probabilities defined in Eq. (25). The values of the quadrupole moments calculated in Nilsson model are shown in Fig. 16 and those for Nilsson-Seo model in Fig. 17. The experimental data (crosses with error bars) were extracted from Refs. [55,56]. The similar results obtained with Nilsson-Seo single particle potential were reported early [6,7] but for the monopole pairing.

VII. CONCLUSIONS

In the present paper we have calculated the basic characteristics of nuclei in the rare earth region using the Nilsson-type potential and the Strutinsky macroscopic-microscopic prescription with the state dependent δ-type pairing force and the LSD macroscopic model.

First, we have adjusted the pairing strength constants V_0 for the considered nuclei and models of interest. The values of V_0 depend on the energy cutoff (such as the traditionally explored G constants in case of the monopole pairing). The typical value of V_0 corresponding to the pairing window which consist of $n=2\sqrt{15N(Z)}$ levels is around 250 MeV fm^3.

Calculating the masses we have used LSD model [27] in which the additional curvature term is added. The masses for the considered set of about 200 nuclei are reproduced with the rms mass deviation equal to 0.700 MeV. For comparison the rms deviation in other calculations such as FRDM [33], ETFSI [23], HFBCS-1 [24] or in the new approach as in Ref. [27] done for nearly 3000 nuclei is less than the given value.

The nuclear radii calculated in the framework of the present model do not differ very much from those obtained in other approaches of this type. The best calculations which reproduce RMSR are the self-consistent Skyrme-HF models. The rms radii are reproduced here with the accuracy defined by rms deviation which is 0.08 fm which is twice higher, e.g., FRDM or four times so large as HFBCS-1 radii [26].

The deformations and the quadrupole moments are comparable to experimental data and consistent with other approaches (see, e.g., Refs. [7,33]).

It is worth mentioning here that the calculation time in case of the state dependent δ pairing does not increase very much in comparison to the calculations with constant matrix elements.

Our aim was to find if the Nilsson models when used with the δ-type state dependent pairing force can reproduce basic nuclear data concerning both deformed and undeformed nuclei. The use of the δ-pairing force instead of the traditional monopole pairing with constant matrix elements seems to work at the similar accuracy as compared to the latter. From the point of view of practical calculations the monopole pairing force still seems to be a satisfactory choice for the residual part of the nuclear interaction.

[1] S. G. Nilsson, Mat. Fys. Medd. K. Dan. Vidensk. Selsk. **29**, 16 (1955).
[2] S. G. Nilsson, C. F. Tsang, A. Sobiczewski, Z. Szymański, C. Wycech, C. Gustafson, I.-L. Lamm, P. Möller, and B. Nilsson, Nucl. Phys. **A131**, 1 (1969).
[3] V. M. Strutinsky, Nucl. Phys. **A95**, 420 (1967).
[4] V. M. Strutinsky, Nucl. Phys. **A122**, 1 (1968).
[5] M. Brack, J. Damgaard, A. S. Jensen, H. C. Pauli, V. M. Strutinsky, and C. Y. Wong, Rev. Mod. Phys. **44**, 320 (1972).
[6] B. Nerlo-Pomorska, K. Pomorski, and B. Skorupska-Mach,

Nucl. Phys. **A562**, 180 (1993).
[7] B. Nerlo-Pomorska and B. Mach, At. Data Nucl. Data Tables **60**, 287 (1995).
[8] W. von Oertzen and A. Vitturi, Rep. Prog. Phys. **64**, 1247 (2000).
[9] R. F. Casten, *Nuclear Structure from a Simple Perspective* (Oxford University Press, New York, 1990).
[10] D. R. Bes and R. A. Broglia, Phys. Rev. C **3**, 2349 (1971).
[11] E. R. Flynn, G. Igo, P. D. Barnes, D. Kovar, D. R. Bes, and R. A. Broglia, Phys. Rev. C **3**, 2371 (1971).
[12] Z. Łojewski, B. Nerlo-Pomorska, and K. Pomorski, Acta Phys. Pol. B **25**, 1147 (1994).
[13] Y. Sun, S. Wen, and D. H. Feng, Phys. Rev. Lett. **72**, 3483 (1994).
[14] W. Satuła and R. Wyss, Nucl. Phys. **A669**, 119 (2000).
[15] S. J. Krieger, P. Bonche, H. Flocard, P. Quentin, and M. Weiss, Nucl. Phys. **A517**, 275 (1990).
[16] W. Pöschl, D. Vretenar, and P. Ring, Comput. Phys. Commun. **103**, 217 (1990).
[17] W. Pöschl, D. Vretenar, G. Lalazissis, and P. Ring, Phys. Rev. Lett. **79**, 3841 (1997).
[18] J. Meng, Nucl. Phys. **A635**, 3 (1998).
[19] A. Baran and W. Höhenberger, Phys. Rev. C **52**, 2242 (1995).
[20] A. Baran and W. Höhenberger, Phys. Rev. C **53**, 1571 (1996).
[21] L. Próchniak, K.Zając, K. Pomorski, S. G. Rohoziński, and J. Srebrny, Nucl. Phys. **A648**, 181 (1999).
[22] Y. Aboussir, J. M. Pearson, A. K. Dutta, and F. Tondeur, Nucl. Phys. **A549**, 155 (1992).
[23] Y. Aboussir, J. M. Pearson, A. K. Dutta, and F. Tondeur, At. Data Nucl. Data Tables **61**, 127 (1995).
[24] F. Tondeur, S. Goriely, J. Pearson, and M. Onsi, Phys. Rev. C **62**, 024308 (2000).
[25] S. Goriely, F. Tondeur, and J. Pearson, At. Data Nucl. Data Tables **77**, 311 (2001).
[26] F. Buchinger, J. Pearson, and S. Goriely, Phys. Rev. C **64**, 067303 (2001).
[27] K. Pomorski and J. Dudek, Phys. Rev. C **67**, 044316 (2003).
[28] W. D. Myers and W. J. Swiatecki, Ann. Phys. (N.Y.) **55**, 395 (1969).
[29] W. D. Myers and W. J. Swiatecki, Ann. Phys. (N.Y.) **84**, 186 (1974).
[30] Z. Łojewski, A. Baran, and K. Pomorski, Acta Phys. Pol. B **34**, 1801 (2003).
[31] W. D. Myers, At. Data Nucl. Data Tables **17**, 411 (1976).
[32] T. Seo, Z. Phys. A **324**, 43 (1986).
[33] P. Möller, J. R. Nix, W. D. Myers, and W. J. Swiatecki, At. Data Nucl. Data Tables **59**, 185 (1995).
[34] J. Berger, M. Girod, and D. Gogny, Comput. Phys. Commun. **63**, 365 (1991).
[35] J. Dechargè and D. Gogny, Phys. Rev. C **21**, 1568 (1975).
[36] R. Sachs, *Nuclear Theory* (Addison-Wesley, Reading, Massachussets, 1953).
[37] T. Otto, G. Bollen, G. Savard, L. Schweikhard, H. Stolzenberg, G. Audi, R. B. Moore, G. Rouleau, J. Szerypo, and Z. Patyk, Nucl. Phys. **A567**, 281 (1994).
[38] M. Anthony, CRN ea Université Louis Pasteur Technical Report 2002.
[39] E. W. Otten, in *Treatise on Heavy-Ion Science*, edited by D. A. Bromley (Plenum, New York, 1989), Vol. 8, pp. 517–638.
[40] E. G. Nadjakov, K. P. Marinova, and Y. Gangrsky, At. Data Nucl. Data Tables **56**, 133 (1994).
[41] C. Batty, E. Friedman, H. Gils, and R. Machleidt, Adv. Nucl. Phys. **19**, 1 (1989).
[42] Z. Łojewski, B. Nerlo-Pomorska, K. Pomorski, and J. Dudek, Phys. Rev. C **51**, 601 (1995).
[43] A. Bohr and B. R. Mottelson, *Nuclear Structure, Single-Particle Motion*, Vol. I (Benjamin, New York, 1969).
[44] K. Böning, A. Sobiczewski, and K. Pomorski, Acta Phys. Pol. B **16**, 393 (1985).
[45] F. Tondeur, Nucl. Phys. **A315**, 353 (1978).
[46] M. Bender, K. Rutz, P.-G. Reinhard, and J. Mahrun (unpublished).
[47] D. G. Madland and R. Nix, Nucl. Phys. **A476**, 1 (1988).
[48] J. Dobaczewski, P. Magierski, W. Nazarewicz, W. Satuła, and Z. Szymański, Phys. Rev. C **63**, 024308 (2001).
[49] W. Press, S. Teukolsky, W. Vettering, and B. Flannery, *Numerical Recipes in Fortran. The Art of Scientific Computing* (CUP, Cambridge, 1992).
[50] G. Audi and A. H. Wapstra, Nucl. Phys. **A565**, 1 (1993).
[51] G. Audi and A. H. Wapstra, Nucl. Phys. **A595**, 409 (1995).
[52] Z. Patyk, A. Baran, J. Berger, J. Dechargé, J. Dobaczewski, R. Smolańczuk, and A. Sobiczewski, Acta Phys. Pol. B **27**, 457 (1995).
[53] Z. Patyk, A. Baran, J. Berger, J. D. J. Dechargé, P. Ring, and A. Sobiczewski, Phys. Rev. C **59**, 704 (1999).
[54] Z. Patyk, A. Baran, J. Berger, J. D. J. Dechargé, P. Ring, and A. Sobiczewski, in *International Conference*, edited by W. Scientific (Dubna, 1998), pp. 497–502.
[55] S. Raman, C. H. Malarkey, W. T. Milner, C. W. J. Nestor, and P. H. Stelson, At. Data Nucl. Data Tables **36**, 1 (1987).
[56] S. Raman, C. W. J. Nestor, S. Kahane, and K. H. Bhat, At. Data Nucl. Data Tables **42**, 1 (1989).